POLITECNICO DI TORINO
Repository ISTITUZIONALE

Advanced Sensorless Control System for PMSM-based Automotive Application

Original
Advanced Sensorless Control System for PMSM-based Automotive Application / VOLA GERA, Luca; Botto, Gianluca; SUAREZ CABRERA, LESTER DANIEL; Chiaberge, Marcello. - ELETTRONICO. - 1:(2014), pp. 1-8. (Intervento presentato al convegno 16th Conference on Power Electronics and Applications, EPE'14-ECCE Europe tenutosi a Lappeenranta - FINLAND nel 26-28 August 2014).

Availability:
This version is available at: 11583/2561805 since:

Publisher:
EPE Association

Published
DOI:

Terms of use:
openAccess

This article is made available under terms and conditions as specified in the corresponding bibliographic description in the repository

Publisher copyright

(Article begins on next page)

04 May 2023

Advanced Sensorless Control System for PMSM-based Automotive Application

Luca Vola Gera, Gianluca Botto, Lester D. Suarez Cabrera and Marcello Chiaberge
POLITECNICO DI TORINO
Corso Duca degli Abruzzi 24, 10129, Torino
Email : luca.volagera, gianluca.botto, lester.suarezcabrera, marcello.chiaberge@polito.it
URL : www.polito.it

Keywords

<<Permanent Magnet Motor>>, <<Sensorless control>>, <<High-speed drive>>, <<Synchronous motor>> , <<Vector control>>.

Abstract

Electrical drives are widely used in industrial applications like energy production, management and recovery. In this paper the control of PM motors for high speed automotive applications is investigated. Here, an improved *DQ* Control with a Sliding Mode Observer is implemented to guarantee high efficiency. As a result, comparisons are made between simulation and experimental test, illustrating the performance of the drive technique and the control design approach.

Introduction

Permanent magnet synchronous motors (PMSM) are widely used in industrial applications due to their intrinsic high precision, dynamics and efficiency. The high power density also makes them very interesting for energy management, production and recovery (for example as kinetic energy recovery systems in the automotive field or flywheels and turbine control for gas production). To control them the angular position is required but sometimes there are no possibilities to have a position sensor in order to detect the motor's position and speed. So an observer is required to obtain position and speed of the shaft. Many methods have been proposed, Kalman Filter[1], Extended Kalman Filter[2]-[3], Mras Method [4], Signal injection[5] and Flux Observer[6]-[7].
In this paper a Sliding Mode Observer[8] with standard quadrature control for high speed motors (over 60000rpm) and working with the minimum possible switching frequency is presented and investigated. In this kind of applications, as the mechanical speed increases (or with many pole pairs) it is mandatory to increase the relative control and PWM switching frequency. For this reason, the motor control with minimum frequency is a great advantage: the target is being able to control motor torque and speed with about 15 points per period. Consequently the switching frequency is only 15 time the electrical rated speed: based on this a lot of effort is dedicated in improving the CPU time required to execute the motor control cycle. A suitable control structure for high speed motor control is analyzed, than the observer structures in presented, and indeed the simulation results and experimental results are presented.

Application in Hybrid Turbocharger

Recently, a new type of application has required the development of electric motors able to reach and exceed 100krpm: the electric or hybrid turbocharger for automotive applications. This system consists in having an electric motor directly connected to the shaft of the turbine compressor block (fig.1) that can be used both for energy recovery, like a turbine generator powered from exhaust gas, and to avoid the turbo lag phenomena: this is possible accelerating the turbine independently of the pressure of the exhaust gas, then regardless the rotation speed of the internal combustion engine. The other big advantage is the possibility, by means of proper sizing, of using the system as a continuous source of power, controlling the speed of the turbine and braking it: the recovered energy can be used to power a electric drive(i.e. power traction).

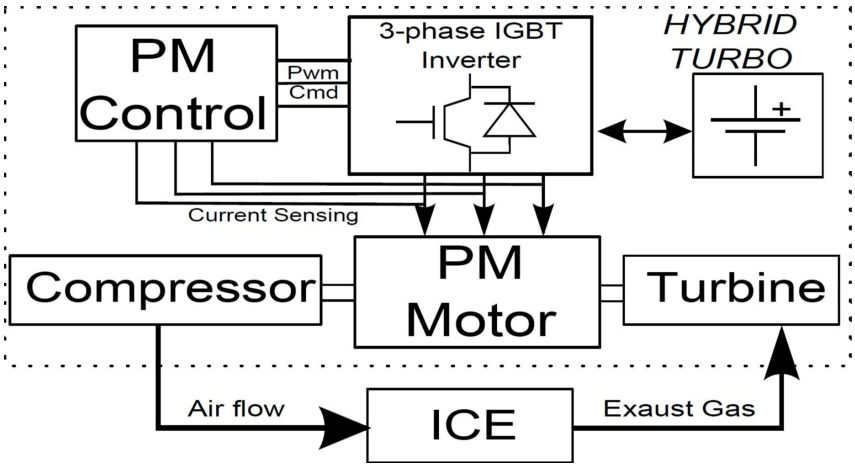

Figure 1: Schematic architecture of a electric turbocharger system.

Motor Model

The mathematical model of PM motor can be described in DQ plane by the following equations (table II for symbols explanation)

$$\begin{cases} v_{sd} = R_s \cdot I_{sd} + L_d \dfrac{dI_{sd}}{dt} - \omega_e \cdot L_q \cdot I_{sq} \\ v_{sq} = R_s \cdot I_{sq} + L_q \dfrac{dI_{sq}}{dt} + \omega_e \cdot L_d \cdot I_{sd} + \omega_e \cdot \lambda_m \\ T_{mech} = 1.5 \cdot p \cdot I_q(\lambda_m - (L_d - L_q) \cdot I_d) \end{cases} \tag{1}$$

The presented model in DQ frame is valid both for isotropic and anisotropic rotors and assuming constant inductances. Transforming the eq.1 in the $\alpha\beta$ plane with the inverse Park transformation the following equations are obtained (eq.2, table II for symbols explanation).

$$\begin{cases} v_\alpha = R_s \cdot I_\alpha + L_{eq} \dfrac{dI_\alpha}{dt} - \omega_e \cdot \lambda_m \cdot sin\theta_e \\ v_\beta = R_s \cdot I_\beta + L_{eq} \dfrac{dI_\beta}{dt} + \omega_e \cdot \lambda_m \cdot cos\theta_e \\ T_{mech} = 1.5 \cdot p \cdot \lambda_m(I_\alpha \phi_\beta - I_\beta \phi_\alpha) \end{cases} \tag{2}$$

The terms $\omega_e \cdot \lambda_m \cdot sin\theta_e$ and $\omega_e \cdot \lambda_m \cdot cos\theta_e$ represent the back EMF, the motor's electromotive force, that include the informations on the rotor position and speed. Using the extended back EMF theory [8]-[9] it is possible to express rotor anisotropy in the $\alpha\beta$ plane, and so to deriver a model where L_d and L_q values and the rotor position appears explicitly (eq.3, table II for symbols explanation):

$$\begin{cases} v_\alpha = R_s \cdot I_\alpha + L_d \dfrac{dI_\alpha}{dt} - \omega_e(L_d - L_q)I_\beta - ((L_d - L_q)(\omega_e I_{sd} - I_{sq}) + \omega_e \lambda_m) sin\theta_e \\ v_\beta = R_s \cdot I_\beta + L_q \dfrac{dI_\beta}{dt} - \omega_e(L_d - L_q)I_\beta - ((L_d - L_q)(\omega_e I_{sd} - I_{sq}) + \omega_e \lambda_m) cos\theta_e \end{cases} \tag{3}$$

Control Structure

A standard quadrature control is used to achieve the speed reference (fig.2). The driver is divided into two different parts: an external one designed to generate current references according to control speed and an internal one with the currents controlled by the proposed sensorless observer.
Working with few control points per period leads to the necessity of adding the following control features in order to improve system efficiency:

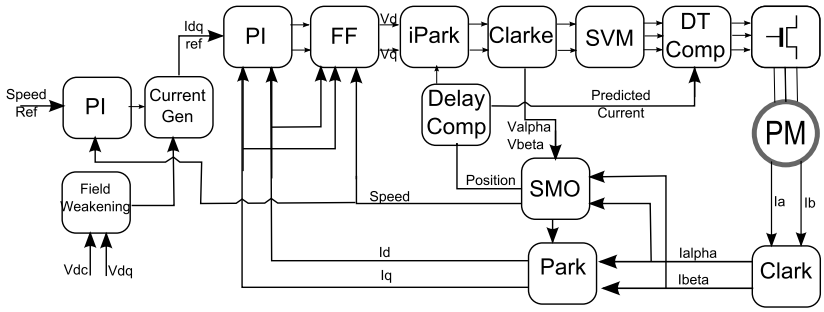

Figure 2: Proposed driver architecture.

Feed Forward

The eq.1 are clearly coupled, with the Id current value present into Iq equation and vice versa, this brings to lower closed loop dynamics so the following (eq.4) term are added to PI current controller output to decouple the two equations.

$$\begin{cases} FF_d = -\omega_e \cdot L_q \cdot I_{sq} \\ \\ FF_q = +\omega_e \cdot L_d \cdot I_{sd} + \omega_e \cdot \lambda_m \end{cases} \tag{4}$$

Inverter Delay Compensation

Discrete control does not take into account the rotor movement: with a low motor speed this phenomenon is negligible but at high speed this is not true. Between two control periods the movement can not be ignored and acting without considering the compensation is like having an error in the resolver offset. Therefore a compensation for rotor movement is required: we can use the actual rotor speed to correct rotor position (eq.5).

$$\theta_{act} = \theta_{est} + k \cdot T_s \cdot \omega_e \tag{5}$$

The value of k is set at 1.5 in order to minimize the error between the position used for duty calculation and real motor position in the next sampling time. The same angular position is used to do a raw estimation of three-phase current in the next sampling period with an inverse Park and Clarke transformation.

Dead Time Compensation

The dead time used to protect the inverter from short circuits, leads to a distortion in current waveforms that can be compensated if the values of phase current are predicted during the sampling time. The raw prediction of phase currents used for this purpose are obtained with position derived with eq.5 and using the Iq and Id reference values via the inverse Park and Clarke transformation ; knowing the currents values in the next sampling time it is possible to predict how the DT will affect the imposed phase voltages and compensate it with a constant a simply rules: a tuned compensation value Δ_{DT} is added or subtracted from the space vector duty output according to the relative phase current sign and value (table I) to minimize the currents waveforms deformation.

Table I: Dead Time Compensation Rule

Iph sign	Comp. Value
> 0	$+\Delta_{DT}$
< 0	$-\Delta_{DT}$

Field Weakening Operation

A flux weakening algorithm is added in the driver structure to achieve motor control over the rated speed or in cases of low values of DC voltage[7]. The applied voltage phasor is compared with the available DC voltage. If duty saturation is detected a PI controller is used to decrease the Id current reference until the saturation disappears. The Iq reference is calculated to obtain a correct torque reference using the standard formula for torque production in IPMSM eq.1.

Sensorless Observer

To detect angular position and speed a proper custom observer is required. Due to his robustness to parameters variation and quite fast execution time, a Sliding Mode Observer is suitable for these applications. The SMO observer is designed starting from the extended back EMF motor model [8] - [9]: the estimated back EMF are used to detect angular position. The observer is based on a current observer that provides an estimation of $I_{\alpha,\beta}$ that are compared to the measured ones, this is even the sliding surface of SMO.
The switching function f starting from the error estimates the motor's back EMF. The common structure of SM implies as switching function the use of the $sign()$ function. To avoid the chattering problem the sign function is substituted by the sigmoid one, in our case the sigmoid function is rawly approximated by a common linear saturation function because in this way is possible to reduce the execution time keeping the same control loop performance. The observer stability has been proved via Lyapunov function, to guarantee stability the gain of the switching function has to be higher than $max(\phi_{\alpha,\beta})$, the maximum amplitude of the motor's back EMF.
A low pass filter is used to filter the estimated back EMF removing high frequency components due to the switching function, then the angular position θ_e is derived from back EMF using the $atan2$ operator. The motor speed is computed from θ_e with a simple derivative operation: another final low pass filter is used to remove derivative noise. There are many other methods to extract position and speed from back EMF like PLL [10] or Kalman filters [1] but these methods require much more maths and so a greater execution time than the chosen one.
The low pass filter on back EMF introduces an intrinsic delay on θ_{est} that has to be compensate, the compensation is simply based on the theoretical phase shift evaluation due to low pass filter introduction:

$$\phi = -atan(\omega_e \cdot \tau) \tag{6}$$

where τ is the filter pole and ω_e is the signal frequency that in this case is coincident with rotor electrical speed. Fig. 3 shows the SM observer structure with the position delay compensation.
Since there is a dead time compensation for the sensorless algorithm, the theoretical reference voltages (not compensated with dead time compensation strategy) of control step $k-1$ are given to the SMO observer in $\alpha\beta$ plane, the same as electric sampled currents (see fig.2) at step k as results of applied voltages.
At high motor speed, the small number of control point are available, but the angular position has to be accurate anyway, so to guarantee the highest precision a Tustin discretization is used instead the common forward Euler.
From the equation 7 it is possible to describe observer dynamics (table II for symbols explanation):

$$\begin{cases} \dfrac{dI_{s\alpha}^{SM}}{dt} = -\dfrac{R_s}{L_d} I_{s\alpha}^{SM} - \omega_e \dfrac{L_d - L_q}{L_d} I_{s\beta}^{SM} + \dfrac{1}{L_d} v_{s\alpha} - f\left(\dfrac{(I_{s\alpha}^{SM} - I_{s\alpha})}{L_d}\right) \\ \dfrac{dI_{s\beta}^{SM}}{dt} = -\dfrac{R_s}{L_{eq}} I_{s\beta}^{SM} - \omega_e \dfrac{L_d - L_q}{L_d} I_{s\alpha}^{SM} + \dfrac{1}{L_d} v_{s\beta} - f\left(\dfrac{(I_{s\beta}^{SM} - I_{s\beta})}{L_d}\right) \end{cases} \tag{7}$$

Simulation Results

A Matlab Simulink model was built to validate the control algorithm using an high speed IPM motor model. The target speed was set to 60krpm with 30kHz switching frequency because of the 2-pole-pairs motor structure: in this way the ratio of 15 control points per electrical period is verified. The control and current reference loop is executed at 2kHz.

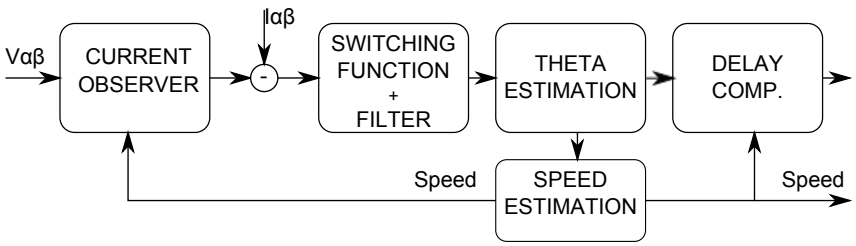

Figure 3: Sliding Mode Observer Structure.

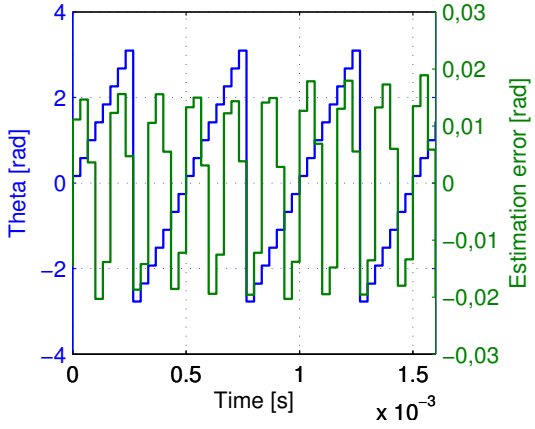

(a) Real position (blue) and estimation error (green).

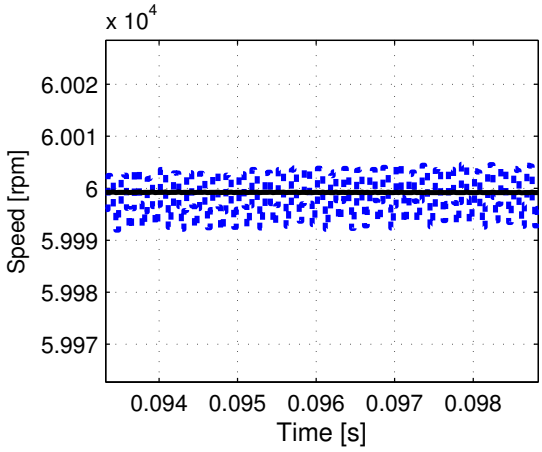

(b) Real speed (black) and estimated speed (blue).

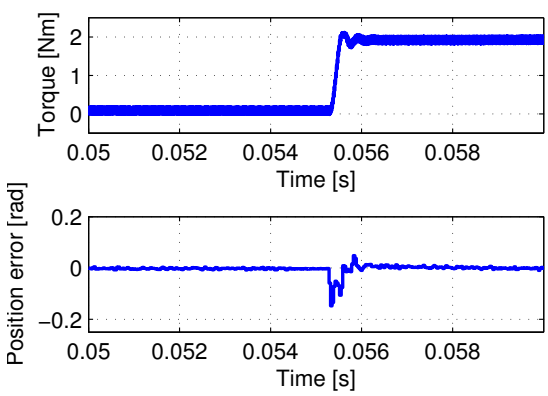

(c) Torque produced and Position error.

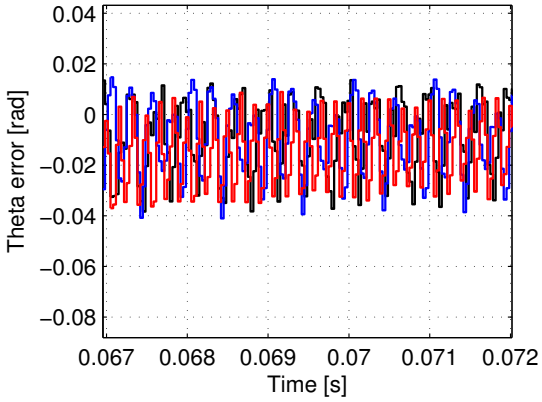

(d) Variation of L_d and L_q 5% (blue), 10% (black), 20% (red).

Figure 4: Simulation Results

Figure 4a shows the precision of the sensorless algorithm: the maximum estimation error is less than 0.02 radians, so less than 1% whereas the motor speed is estimated without significant error in steady state condition (fig.4b).
In fig.4c it is possible to see 2Nm motor torque step sensorless control response at 60krpm and the position error, controlling the motor with the estimated theta, is less than 0.2 radians in correspondence of torque step. The robustness of the proposed observer is tested in simulation detuning the motor inductances values; the results are showed in fig.4d with 15 point per control period.

Experimental Results

The proposed algorithm was initially tested on a small custom testbench (fig.5) in order to demonstrate coherence between simulations and real performances. The testbench is based on a 2 poles, 250W high speed SPMSM motor with a target speed of 60krpm: the switching frequency was set at 15kHz to have exactly 15 point per control period at the maximum motor frequency; other test are done at 30kHz, 50kHz and 70kHz; the increasing of control point brings to better observer's behavior(in terms of position error). The control platform and the power driver used for the experiment are fully developed at the Politecnico di Torino Mechatronics Lab[11]: the system is a general purpose automotive actuating control unit (ACU) designed around a six-leg power stage with high switching frequency capability (up to 100kHz).
The power stage is based on six high speed IXYS full leg MOSFET devices tha can be driven and/or configured independently obtaining different power stage architecture (6 independent legs, 3 H-bridges or 2 three-phase power stages) and the dead time is only 250ns. The above control logic board is based on Texas Instrument F28335 floating point DSP running a specific RTOS designed for this kind of demanding applications (fig.5a).
The experimental tests were done at 50% of motor torque capabilities with constant and time-varying

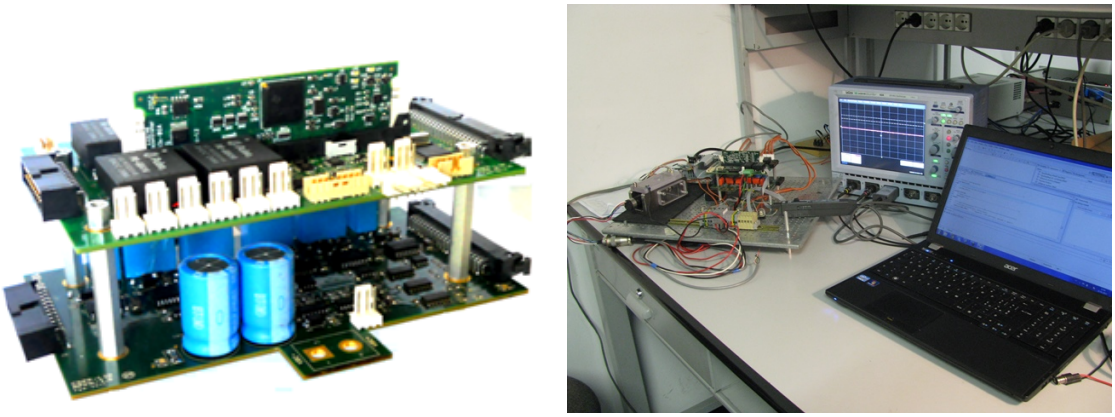

(a) MPPM - Multi Purpose Power Module (b) Custom test bench validation

Figure 5: MPPM Custum Test Bench

speed profiles. Fig.6a represents the SMO estimation error versus the measured θ_e: with a reference speed of 50krpm the maximum error is less than 0.03 radians that means less than 1%; These results are obtained using the estimated speed and position to control the motor. From fig.6b it is possible to evaluate the speed estimation accuracy using a time varying speed reference and with low and high system dynamics. The mismatch error is less than 1%.
The validation campaign on the testbench was also largely dedicated to code validation on the control platform and computing time issues verifications before move the complete sensorless control system and SMO observer on the final real application.
After the fast prototyping and test phase on custom MPPM test bench, the control algorithm and the related developed control code has been deployed on the target application. In final application power module is a custom power module IGBT based, and the DSP used for control is not the previous but a 300MHz floating point to guarantee the correct sensorless control execution even at 100kHz switching frequency, in this case the entire current control loop is executed in less than 1200 instruction, less than 4μs.
In fig.6c it is shown the ability of the proposed control scheme to reach the speed target of 90krpm with applied load torque disturbance just after the end of the open loop startup without oscillation and steady state error. The startup procedure ends at 10krpm; when the reference speed approaches the 0 speed at turn off the control is disabled. In fig.6d there is the control system response to 2Nm torque step at 60krpm(Iq sampled at 200Hz, T measured with torquemeter, Id not shown), in both cases it is not possible to check error position as in fig.6c because the position sensor is not available on real motor applications so the validation of sensorless control is based on torque measurement end efficiency analysis. The average torque production respect to the theoretical torque is only 1%.

Startup Procedure

Since the SMO sensorless observer is based on motors back EMF, the control algorithm is not able to start at zero speed: for this reason, and due to the special type of the target application, the closed loop startup is not required; there is no braking torque and the turbine speed is never zero, so an open loop procedure is required to start the control system. An I/f method is used: the control system requires a time varying current profile using a fake created angular position. When the constant acceleration startup procedure reaches the target speed for sensorless commutation, the speed estimation state switches to closed loop sliding mode sensorless control.
During startup procedures the required torque/current value is not constant but it has an higher value in order to contrast friction: no constant current with fixed theta was used to align rotor with a specific motor phase. During startup the reference speed is ignored and the sensorless startup procedure starts independently from reference.
The commutation speed between open and closed loop procedures is about 5-10% of motor rated speed. For the real application motor used during experimental test the proper speed for commutation is about 11krpm with $3000 rpm/s^2$ of acceleration; the motor start with less than 5% of rated torque. In fig.6e it is shown the whole startup process.

Conclusions

A complete modeling, simulation, validation and testing design flow for high speed high power PMSM motor sensorless control is presented in this article. The proposed control structure has been developed through several steps at the Mechatronics Lab Politecnico di Torino in collaboration with Magneti Marelli

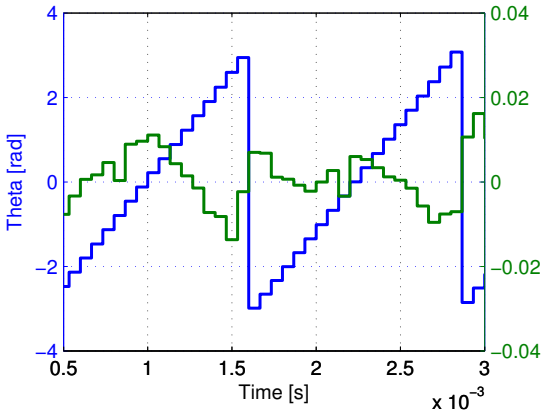

(a) Real position (blue) and sensorless position error (green).

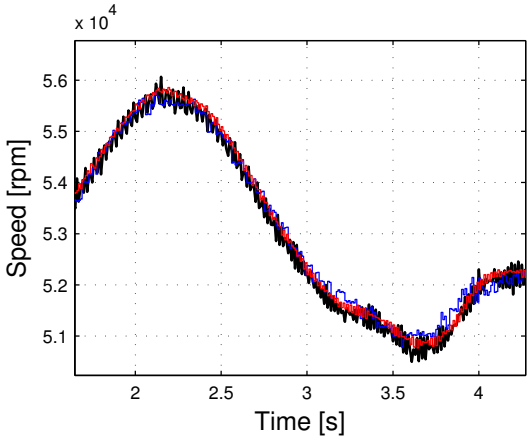

(b) Real speed (black), estimated speed (red) and reference speed (blue).

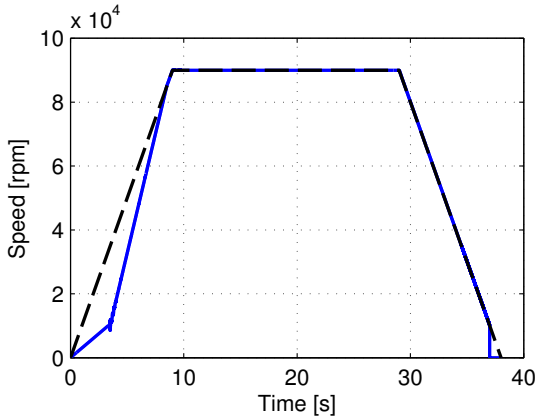

(c) Speed control : reference (black) and estimated motor speed(blue).

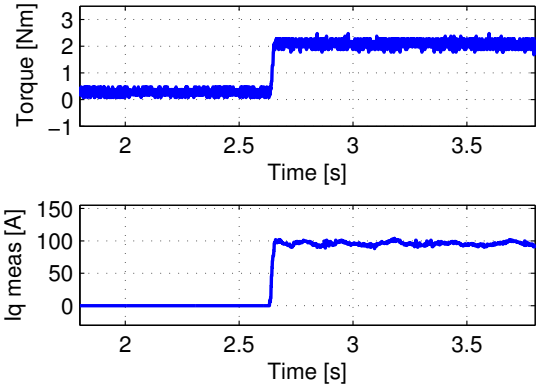

(d) Torque step : produced torque and measured I_q.

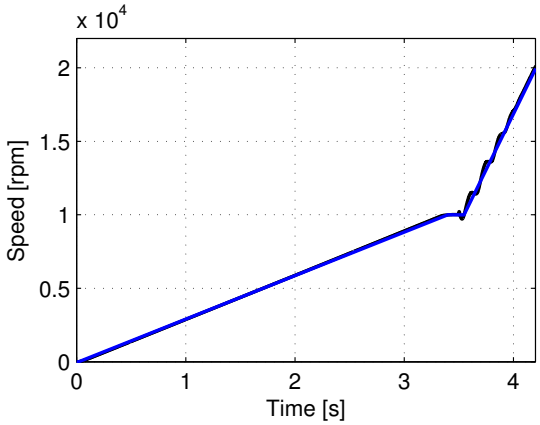

(e) Startup process, estimated speed (black) and reference speed (blue).

Figure 6: Experimental Results

(MM). The developed SMO observer is stable, and capable of generating the required performances even beyond the mechanical 100krpm with only 15 control points per rotation period.

Table II: List of symbols used.

$v_{sd,sq}$	dq Stator voltages
$v_{\alpha,\beta}$	$\alpha\beta$ Stator voltages
$I_{sd,sq}$	dq Stator currents
$I_{\alpha,\beta}$	$\alpha\beta$ Stator currents
$I^{SM}_{s\alpha,s\beta}$	*SM* Estimated currents
R_s	Stator resistance
$L_{d,q}$	Motor dq inductance
L_{eq}	Motor $\alpha\beta$ inductance
ω_e	Electrical speed
θ_e	Electrical position
θ_{est}	Electrical position estimated
$\phi_{\alpha\beta}$	$\alpha\beta$ Magnet flux
λ_m	Magnet flux linkage
p	Motor pole pairs
T_{mech}	Motor produced torque
$FF_{d,q}$	Feed forward compensation d,q
T_s	Sampling time

References

[1] M.C. Huang, A.J.Moses, F.Anayi and X.G. Yao, *Linear Kalman Filter(LKF) Sensorless Control for Permanent Magnet Synchronous Motor Based on Orthogonal Output Model*, International Symposium on Power Electronics, Electrical drives, Automation and Motion, 2006.

[2] S.Bolognani, L.Tubiana M.Zigliotto,*EKF-Based Sensorless IPM Synchronous Motor Drive for Flux-Weakening Applications*, IEEE TRANSACTIONS ON INDUSTRIAL ELECTRONICS, VOL. 39, NO. 3, JUNE 2003.

[3] S. Bolognani, R. Oboe and M. Zigliotto, *Sensorless Full-Digital PMSM Drive With EKF Estimation of Speed and Rotor Position*, IEEE TRANSACTIONS ON INDUSTRIAL ELECTRONICS, VOL. 46, NO. 1, FEBRUARY 1999.

[4] Y. S. Kim, S. K. Kim and Y. A. Kown, *MRAS Based Sensorless Control of Permanent Magnet Synchronous Motor*, SICE Annual Conference in Fukui, 2003. Fukui University, Japan

[5] J. Lara;A. Chandra,J. Xu , *Integration of HFSI and extended-EMF based techniques for PMSM sensorless control in HEV/EV applications*, IECON 2012 - 38th Annual Conference on IEEE Industrial Electronics Society.

[6] M. Rashed, P. MacConnell, A. Fraser Stronach, and P. Acarnley, *Sensorless Indirect-Rotor-Field-Orientation Speed Control of a Permanent-Magnet Synchronous Motor With Stator-Resistance Estimation*, IEEE TRANSACTIONS ON INDUSTRIAL ELECTRONICS, VOL. 54, NO. 3, JUNE 2007.

[7] Genduso, F. ; Miceli, R. ; Rando, C. ; Galluzzo, G.R,*Back EMF Sensorless-Control Algorithm for High-Dynamic Performance PMSM*, IEEE TRANSACTIONS ON INDUSTRIAL ELECTRONICS, VOL. 57, NO. 6, JUNE 2010.

[8] D. Jiang, Z. Zhao and F. Wand, *A Sliding Mode Observer for PMSM Speed and Rotor Position Considering Saliency*, Power Electronics Specialists Conference, 2008.

[9] A. Eilenberger and M. Schroedl, *Extended back EMF model for PM synchronous machines with different inductances in d- and q-axis* Power Electronics and Motion Control Conference, 2008.

[10] S. Bolognani, S. Calligaro and R. Petrella, *Design Issues and Estimation Errors Analysis of Back-EMF Based Postion and Speed Observer for SPM Synchronous Motors*, Symposium on Sensorless Control for Electrical Drives (SLED), 2011.

[11] A. Bonfitto, G. Botto, M. Chiaberge, L.D. Suarez, A. Tonoli, *A multi-purpose control and power electronic architecture for active magnetic actuators*,15th International Power Electronics and Motion Control Conference, EPE-PEMC 2012.

[12] P.V. Medagam, T. Yucelen, F. Pourboghrat, *Adaptive SDRE-Based Nonlinear Sensorless Speed Control for PMSM Drives*,39th North American Power Symposium, 2007. NAPS '07.

[13] Pellegrino, G. ; Armando, E. ; Guglielmi, P. ,*Direct Flux Field-Oriented Control of IPM Drives With Variable DC Link in the Field-Weakening Region*, IEEE TRANSACTIONS ON INDUSTRY APPLICATION, VOL. 45, NO. 5, JUNE 2009.

[14] Vola Gera, L.; Botto G.; Suarez Cabrera L.; Chiaberge M. ,*Sensorless Control Design for High-speed / High-power PMSM-based Automotive Application* , EE 2013, Novi Sad, Serbia.